Tensile mechanical properties of the cervical, thoracic and lumbar porcine spinal meninges

Arthur Jourdan, Arnaud Le Troter, Pierre Daude, Stanislas Rapacchi, Catherine Masson, Thierry Bège, David Bendahan

Tensile Mechanical Properties of the Cervical, Thoracic and Lumbar Porcine Spinal Meninges

Patrice SUDRES (1,4), Morgane EVIN (1,4), Eric WAGNAC (2,3,4), Nicolas BAILLY (2,3,4), Lucien DIOTALEVI (2,3,4), Anthony MELOT (1,4,5), Pierre-Jean ARNOUX (1,4), Yvan PETIT (2,3,4)

1. *Laboratoire de Biomécanique Appliquée, UMRT24 AMU/IFSTTAR, Marseille, France.*
2. *Department of Mechanical Engineering, École de Technologie Supérieure, 1100 Notre-Dame Street West, Montréal, Québec H3C 1K3, Canada*
3. *Research Center, Hôpital du Sacré-Coeur de Montréal, 5400 Gouin blvd, Montréal H4J 1C5, Québec, Canada*
4. *iLab-Spine – Laboratoire International en Imagerie et Biomécanique du Rachis, Marseille, France & Montréal, Canada.*
5. *Hôpital privé Clairval, Marseille, France.*

Corresponding author: *Morgane EVIN*

Address:

Laboratoire de Biomécanique Appliquée

IFSTTAR/Université Aix-Marseille

UMR T24

Faculté de Médecine Nord

Boulevard Pierre DRAMART

13016 MARSEILLE CEDEX 20

Tel: (00 33) 4 91 65 80 06

Fax: (00 33) 4 91 65 80 19

E-Mail: morgane.evin@univ-eiffel.fr

Keywords: meninges, mechanical properties, biomechanics, spine, elasticity

Abstract:

Background. The spinal meninges play a mechanical protective role for the spinal cord. Better knowledge of the mechanical behavior of these tissues wrapping the cord is required to accurately model the stress and strain fields of the spinal cord during physiological or traumatic motions. Then, the mechanical properties of meninges along the spinal canal are not well documented. The aim of this study was to quantify the elastic meningeal mechanical properties along the porcine spinal cord in both the longitudinal direction and in the circumferential directions for the dura-arachnoid maters complex (DAC) and solely in the longitudinal direction for the pia mater. This analysis was completed in providing a range of isotropic hyperelastic coefficients to take into account the toe region.

Methods. Six complete spines (C0 – L5) were harvested from pigs (2-3 months) weighing 43 +/- 13 kg. The mechanical tests were performed within 12h *post mortem*. A preload of 0.5N was applied to the pia mater and of 2N to the DAC samples, followed by 30 preconditioning cycles. Specimens were then loaded to failure at the same strain rate 0.2 mm/s (approximately 0.02/s, traction velocity/length of the sample) up to 12 mm of displacement.

Results. The following mean values were proposed for the elastic moduli of the spinal meninges. Longitudinal DAC elastic moduli: 22.4 MPa in cervical, 38.1 MPa in thoracic and 36.6 MPa in lumbar spinal levels; circumferential DAC elastic moduli: 20.6 MPa in cervical, 21.2 MPa in thoracic and 12.2 MPa in lumbar spinal levels; and longitudinal pia mater elastic moduli : 18.4 MPa in cervical, 17.2 MPa in thoracic and 19.6 MPa in lumbar spinal levels.

Discussion. The variety of mechanical properties of the spinal meninges suggests that it cannot be regarded as a homogenous structure along the whole length of the spinal cord.

Abbreviations

DAC: dura-arachnoid mater complex

PM: pia mater

ROI: region of interest

DIC: digital image correlation

CSA: cross-sectional area

GUM: Guide to the expression of Uncertainty in Measurement

SE : standard error

SD: standard deviation

RMSE (Root Mean Square Error).

ROM: range of motion

CSF: cerebrospinal fluid

1. Introduction

The spinal meninges composed of the dura mater, the arachnoid mater and the pia mater, play a mechanical protective role for the spinal cord (Sakka et al. 2016). The dura mater is a fibrous, white, thick, and resistant membrane formed by a dense connective tissue poorly vascularized with a ratio of collagen I fibers to elastin fibers varying radially. The arachnoid mater can be described as an outer layer, consisting of a thin transparent membrane mainly composed of collagen and elastin fibers, attached to the dura mater by thin strands of collagen. The pia mater is mainly composed of predominantly longitudinally orientated collagen fibers, which carry larger branches of the spinal vasculature (Reina et al. 1997, 2020).
As any biological soft tissue, meningeal mechanical properties are altered *post mortem* due to drying and the interruption of blood supply, thus leading to tissue degeneration (Garo et al. 2007, Fountoulakis et al. 2001). In consequence, the experimental testing methodology needs an thorough management of time and manipulation to provide reliable mechanical measurements in order to highlight the specificities of such biological soft tissues. Better knowledge of the mechanical behavior of these tissues wrapping the cord is required to accurately model the stress and strain fields of the spinal cord during physiological or traumatic motions (Bertram and Heil 2016, Fradet et al. 2016, Sparrey and Keaveny 2009, Kimpara et al.2006, Khuyagbaatar et al. 2014). Such modeling tools allowed the correlation of the stresses fields in the spinal cord with clinical analyses (Lévy et al. 2020, Czyż et al. 2012), and the assessment of the effect of a specific surgery on these tissues (Henao et al. 2016).

The spinal dura mater was mainly tested in tension at different locations of the spine. A porcine cervical cartography of the mechanical properties showed differences between the dorsal and the ventral side of the dura mater (Mazgajczyk et al. 2012). A significant variability of properties was found between species, such as rats (Maikos et al . 2008), dogs (Patin et al. 1993), sheeps (Shetye et al. 2014), swines (Mazgajczyk et al. 2012), cattle (Runza et al. 1999) and humans (Runza et al. 1999, Chauvet et al. 2010). Due to ethical and logistical complications related to human species, the high similarity of porcine model to the human species on the genetic, anatomical, physiological, pathophysiological [Schomberg et al. 2017], and biomechanical [Wilke et al. 2011] levels, the swine model appears as the best transversal human models, next to non-human primates [Schomberg et al. 2017], and is increasingly used in spine research [Kim et al.2019, Ramo et al. 2018b, Brummund et al. 2017, Fradet et al. 2016, Swnindel et al. 2013]. In addition, similarities between human and porcine models were highlighted histologically for the dura mater (3 dural layers structure) [Kinaci et al. 2020].

An anisotropic behavior (in longitudinal or cranio-caudal direction and in circumferential direction) was also reported in most of the species except for the dog. One biaxial study confirmed this difference between these two mechanical orientations on ovine samples (Shetye et al. 2014). The anisotropic behavior was corroborated by histological studies describing, in particular, the longitudinal direction of fibers along the cord (Maikos et al. 2008, Chauvet et al. 2010). Among these studies, the spinal arachnoid mater was considered as a part of the spinal dura mater, excepted for two of them which assumed its adherence to the spinal pia mater (Fabris et al. 2019, Ramo et al. 2018c). The spinal arachnoid-dura tissue

continuity assumption was validated by others histological quantification, showing the arachnoid mater to be the inner layer of the dura mater. The relative thickness of dura-to-arachnoid mater however suggested a limited role of the arachnoid to the mechanical properties of the dura mater (Vandenabeele et al . 1996, Reina et al. 1997). Then, quantification of the mechanical properties of pia and dura-arachnoid mater complex (DAC) mechanical properties is not fully described along the whole spinal cord in the literature. One study compared biomechanical properties of the ovine dura mater at six spinal levels (C_6, C_7, T_{11}, T_{12}, L_4, and L_5). No significant difference of elastic moduli values between longitudinal and circumferential directions at the cervical levels were notified, but this study showed that the ratio between the longitudinal and circumferential elastic moduli were significantly smaller at the cervical and thoracic levels (Yang et al. 2019). In addition, Mazgajczyk et al. (2012) highlighted a significative variability of DAC mechanical properties along the porcine cervical segment between the dorsal and the ventral sides on porcine models. Our hypothesis is that the elastic mechanical properties, which vary between the ventral and dorsal sides, could also vary along the whole longitudinal spinal cord from the spinal cervical to the spinal lumbar levels.

The effect of conservation methods on mechanical characteristics is not systematically quantified. Freezing method at -4°C was shown to modify the mechanical properties variability of the human dura mater through time, while the mechanical properties of the bovine dura mater decreases independently of the time (Runza et al. 1999).

Concerning the spinal pia mater, two studies provided indirect measurements of the cervical compressive and tensile mechanical properties on rabbits (Ozawa et al. 2004) and on human spinal cord (Mazuchowski and Thibault 2003). More recently, quasi-static tensile tests and a dynamics mechanical analysis were performed on cervical ewe pia mater assumed as an integrally laminated structure composed of the arachnoid and the pia maters. This study highlighted the non-linear viscoelasticity of the ewe pia-arachnoid structure (Ramo et al. 2018c).

The aim of this study is to quantify the elastic meningeal mechanical properties along the porcine spinal cord in the longitudinal (cranio-caudal) direction and in the circumferential (surrounding the spinal cord) directions for the DAC, and solely in longitudinal direction for the PM. A quasi-static loading close to physiological solicitations was considered. In addition, the effect of the conservation method effect was assessed by comparing flash frozen (at -80°C) (Sparrey et al. 2009) (different from a classical freezing at -4°C) and fresh samples properties.

2. Material & Methods

2.1. Samples preparation

Two tissue structures were characterized in this study: the dura-arachnoid mater complex (DAC) and the pia mater (PM). Six complete spines (C0 – L5) were harvested from pigs (race: crossbreeding Yorkshire x Landrace, age: 2-3 months, weight: 43 +/- 13 kg, gender: 4 males and 2 females) one to two hours following euthanasia. The animals were euthanatized for reasons unrelated to this study. The spine was firstly extracted by a dissection on the dorsal side using scalpels and oscillating saw. This step was performed less than 35 minutes after euthanasia. The spine was then sectioned in three levels: cervical level (from the foramen magnum to the T1-T2 joint), thoracic level (from the T1-T2 joint to the T13-T14 joint, and lumbar level (from the T13-T14 joint to the L6-S1 joint). The spinal cord-meningeal complex, including the DAC, was carefully removed from the spinal canal through fine dissection with scalpels and gouge clamps, and small clamps (duration of 1 hour). The nerve roots and the denticulate ligaments were resected along the DAC. The spinal cord-meningeal complex from two spinal levels over three were stored in PBS at 4°C. The DAC and PM samples were prepared and tested within a 12 hours and 30 minutes after euthanasia. The remaining one third of spinal cord-meningeal complex was saved using flash-freezing (FF) method at -80°C [Sparrey et al. 2009] and thawed at 4°C and prepared and tested at 20°C. For all samples, the DAC was longitudinally incised on the lateral side of the spinal cord-meningeal complex and was removed from the cord. The same operation was done for the PM, which was also taken apart from the white and grey matters. All the fresh and FF samples were stored in PBS at 20°C to keep them moist after preparation and tested at room laboratory temperature of 20°C.The samples were placed between two pieces of sandpaper into which a window was cut, and a stochastic pattern of dots was applied using an oil-based black paint spray (Ptouch 2x + sspr 6pk flat black, Rust-Oleum Corporation, USA), (Fig 1 – A). This step was used to measure the length and the width of the sample as well as to perform strain and stress fields analyses. The support was then inserted and fastened into the clamps of the testing machine (GRIP ASST, T/C, 3200, Bose Corporation, Framingham, Massachusetts, US). The lateral side of the sandpaper support was cut before testing to allow traction with the clamps (Fig 1 – B). Two different orientations of clamping were used, leading to 2 different loading directions for the DAC: longitudinal and circumferential. PM samples were only tested in the longitudinal direction.

The length (L_0) of the samples was defined as the minimum distance between the clamps at the initial position before testing. The width (w) was defined as the lateral distance of the clamped sample at the initial time position before the mechanical test. Samples not fully attached samples to the clamps [Fig. C.4] or with a visible deterioration after attachment were excluded from the study. The reference thicknesses (t) of the DAC and PM were measured at 3 spinal levels (cervical, thoracic and lumbar) on an additional porcine subject to avoid damaging the samples due to supplementary manipulations. The DAC and PM samples were sectioned to a width of 1mm and a length corresponding to the longitudinal distance between two nerves roots. They were positioned on a black 120g paper. The samples' side with the largest area were glued on with the black paper by a

transparent agar substrate. Then, the samples were positioned on the edge on a graph paper. A Micro C110 camera (Vision Research, 8GB) with a 105 macro lens (Nikon F2.8), as well as two light systems (LED EFFILUX) were used to acquire high resolution images of the samples' thickness. Three samples were sectioned in three sub-samples at each spinal level as defined in the first paragraph of this section. Calibration of the camera was performed using three measurements of the graph paper. Ten measurements were performed on each sub-sample. A total of 30 measurements by tissue (DAC and PM) and by spinal level (cervical, thoracic and lumbar) were performed. The cross-section area (CS*A*) of the sample was assumed to be rectangular and defined as the product of the width (*w*) by the thickness (*t*).

2.2. Tensile Testing

Both types of sample were submitted to the same testing protocol with specific preload and threshold values for the pre-cycling phase. A preload of 0.5 N was applied for the pia mater and of 2 N for the DAC samples followed by 30 preconditioning cycles (frequency varies with the time to reach the preload, the magnitude: 1 N). They were performed to compensate the retraction of the sample and remove any buckling of the sample before testing. The amplitude of preloading was based inthe literature [Shetye et al. 2014, Ramo et al. 2018a,b,c]. A moderate tensile ramp at 0.2 mm/s was chosen in accordance with *in vivo* experiment of porcine spinal-cord-pia-arachnoid construct [Ramo et al. 2018b] and reported by the literature for ex vivo ovine dura mater and pia-arachnoid complex [Ramo et al. 2018a, c].

The tests were stopped at failure or when the maximum displacement was reached (Fig. 2, TableB.1. in Appendix B).

2.3. Data acquisition

A testing machine Bose© ElectroForce 3200 Series (Bose Corporation, Framingham, Massachusetts, US) was used to perform tensile tests (Fig.1).The loads data were acquired with a 22 N load cell (reliability manufacturer error of 0.11 % and a repeatability error of 0.19 %) at a sampling rate of 100 Hz. Dimensions (length and width) as well as the displacements of the samples. Complementary displacement and strain fields were measured by 2D digital image correlation (DIC) (ARAMIS 5 M, GOM mbH, Germany) at 15 frames per second.

2.4. Data analysis

Linear elasticity

The force/displacement curves were zeroed for comparison by subtracting the minimum measured displacement to the initial measured displacement. Each engineering stress-strain curve was computed from the measured force/displacement curves as follows:

$$\sigma = F/CSA \quad \text{Eq. (1)}$$

$$CSA = t * w \quad \text{Eq. (2)}$$

$$\varepsilon = \Delta L/L_0 \quad \text{Eq. (3)}$$

where equation (1) defines the engineering stress (σ) as the ratio of the tensile force (F) over the initial the cross-sectional area (CSA) on which the force is applied. The initial cross-sectional area (Eq.2) of the sample is the product of its thickness (t) by its width (w) in his undeformed state. Equation (3) allows computing the engineering strain (ε) as the ratio of the measured displacement (ΔL) over the initial length (L_0) of the sample.

Three regions of interest (ROI) were identified on force/displacement curves to performed the post-processing of the stress/strain curves. The toe region (ROI 1 in Fig.3) corresponds to a non-linear region before the linear region (region 2 in Fig.3). The elastic limit is defined as the maximum stress point in the linear region. The third region follows the elastic limit and corresponds to a non-linear region called damage region (ROI 2 in Fig.3). The beginning of the damage region was defined by the first observed macroscopic drop in the force-displacement curve even if fiber ruptures could be present before this non-linear ROI. Several others local damage sub-regions describing a progressive, in stages, load loss linked with the progressive in stages rupture. To determine the range of the linear region, the second derivative of each force/displacement curve was computed and the maximum and the minimum inflection points were identified. The maximum and the minimum values of the second derivative were found and projected on the force/displacement curves to establish the elasticity region by two points corresponding to the stress/strain curve as follows. The toe stress (σ_{toe}) and strain (ε_{toe}) represent the values of the first elastic limit point and the damage stress (σ_{damage}) and strain (ε_{damage}) represent the values of the second elastic limit point (Fig. 3). A linear regression was computed between the elastic limits (R^2>0.99 for 111 over 119 fresh samples, and 21 over 22 flash freezing samples). The elastic moduli were computed from the linear regression defining equations (1), (2) and (3). A comparison of elastic moduli between the fresh and flash-frozen samples was performed only for the thoracic spinal samples. This choice was made to avoid the inter-level spinal variability of the samples.

Hyperelasticity

A isotropic hyperelastic one-degree Ogden model was fitted on each experimental curve depicted on Fig. 4. The uniaxial stress-stretch Ogden function is expressed as :

$$\sigma = \frac{2\mu}{b}\left(\lambda^{b-1} + \lambda^{\frac{-b}{2}-1}\right) \qquad \text{Eqt.4}$$

Where μ is the shear modulus and b is a material constant and the stretch ratio defined as λ = ε + 1. The curve fitting was performed with the nonlinear least squares method using the fit function in Matlab R2018b (MatWorks, Natick, MA, USA) and evaluated evaluated by a R^2 and RMSE (Root Mean Square Error).

2.5. Statistical analysis

The uncertainty of samples' CS*A*, and its effect on the linear modulus, due to the use of a sample thickness estimated from a different animal, was evaluated. This uncertainty evaluation was based on the ISO 98:1995 Guide to the Expression of Uncertainty in Measurement (GUM) (ISO 98:1995 GUM) and used the Monte-Carlo simulation approach described in the GUM supplement 1 (JCGM 101:2008).

The model of surface uncertainty is defined as presented in equation (4), where u_S is the uncertainty of the surface value, $u_{w_{rep}}$ is the uncertainty induced by the repeatability of width measurements, $u_{w_{resolution}}$ is the uncertainty induced by the DIC resolution to measure the width, and u_{th_rep} is the uncertainty induced by the repeatability of thickness measurement.

$$u_S = \left(u_{w_{rep}} + u_{w_{resolution}}\right) * u_{th\_rep} \quad \text{Eq.(4)}$$

An algorithm (Solaguren-Beascoa Fernandez et al. 2009) was used with the following input distributions:

- $u_{w_{rep}}$ was defined as a normal distribution from the mean of and the standard deviation (SD) of $w_{measures}$.
- $u_{w_{resolution}}$ was defined as a uniform distribution from -$DIC_{resolution}$ to +$DIC_{resolution}$.
- u_{th_rep} was defined as a normal distribution from the mean of and the standard deviation (SD) of $th_{measures}$.

$w_{measures}$ represents all the width measurements by type of tissue and by spinal level, $w_{resolution}$ represents the resolution of the DIC, and th_{rep} represents all the thickness measurements by type of tissue and by spinal level.

Then, a probabilistic range of linear modulus is provided based on the 32th and the 68th percentile values of the measurement CSA distribution for each sample, corresponding to the most likely physical confidence interval. Then the 32th and the 68th probabilistic value of elastic modulus were calculated from the 32th and the 68th probabilistic value of the CSA. The Monte-Carlo GUM methodology is described in appendix A.

All data were statistically analyzed as follows. The normality of each distribution was verified using Shapiro-Wilk normality tests. Due to the heterogeneity of normal distribution and the unequal distribution size, Wilcoxon rank sum test was performed to quantify the significant difference of all variables (force, stress, displacement, strain, elastic modulus) with respect to the spinal levels, the orientation of loading for the DAC as well as the conservation methods. The significance level was set to $p<0.05$. Data analysis was performed using Matlab software (R2018a version, Matlab®MathWorks,1984). Additionally, Bayesian linear mixed models (blme package - https://github.com/vdorie/blme) were fitted with R [R Core Team 2018] to assess the dependency of our result to the subjects and computed the standard errors (SE) of the elastic modulus taking into account the between-subjects and within-subjects variabilities [Tirrell et al. 2018].

3. Results

The description of fresh and flash-frozen samples which were tested, excluded and analyzed is summarized in Table 1. The exclusion criteria are the following: sample damaged before being fastened into the clamps, sample not well fastened in the clamps, issue due to an operator error with the control command of the computer. Ten fresh samples (0 from longitudinal DAC, 6 from circumferential DAC, 4 from longitudinal pia mater) and 3 flash-frozen samples (0 from longitudinal DAC, 2 from circumferential DAC, 1 from longitudinal pia mater) tore at the middle of their length. All experimental tests were completed less than 12 hours and 30 min after euthanasia of the animal (mean: 7 h 26 min; max: 12 h 23 min).

The dimension of samples from the experimental measured are depicted in Table 2. The samples' range of length is between 8.33 mm and 15.49 mm for the longitudinal DAC while it is between 6.36 mm and 18.51 mm for the circumferential DAC. The range of length is between 6.23 mm and 13.91 mm for the longitudinal PM samples. The DAC sample harvested at the thoracic level are the thickest (0.28 mm) while it is the cervical level for the PM (0.22 mm). The sample's CSA is the greatest at the thoracic levels for the longitudinal and circumferential DAC and the longitudinal PM (with a mean value of 3.77 mm^2, 4.84 mm^2 and 2.44 mm^2 respectively).

Figure 4 reports the corridor of mechanical properties of the fresh samples: the DAC and the PM behavior in longitudinal direction and the DAC behavior in the circumferential direction. The lower and upper curves describe the experimental corridor (shaded area) defining the range from minimum and maximum engineering stress/strain curves. Solid curves represent the typical stress/strain curve.

The elastic modulus of DAC in the longitudinal direction was found to be significantly different between the cervical level (22.35 ± 10.0 MPa) and the two others levels, thoracic (38.1 ± 12.6 MPa) and lumbar (36.6 ± 12.6 MPa). The elastic limit or damage stress/strain point of the cervical samples (0.25 ± 0.09) is 1.7 times superior when compared to the thoracic samples (0.15 ± 0.09), and 1.4 times inferior than the lumbar samples (0.18 ± 0.09). The elastic limit (damage strain) of the circumferential lumbar samples (0.32 ± 0.14) is 1.5 times superior than for the thoracic samples (0.21 ± 0.08) and 1.4 times superior than the cervical samples (0.23 ± 0.1). Elastic modulus of the thoracic samples (21.2 ± 3.0 MPa) is 1.7 times superior than lumbar samples (12.2 ± 4.4 MPa) and slightly superior than cervical samples (20.6 ± 8.1 MPa). Significant differences were found between longitudinal and circumferential elastic moduli between the thoracic (38.1 ± 12.6 MPa against 21.2 ± 3.0 MPa respectively) and lumbar spine (36.6 ± 12.6 MPa against 12.2 ± 4.4 respectively) samples, but not with the cervical samples (Table 3). No significant difference was found between the fresh samples and the flash frozen samples for the DAC (Table 4).

No significant difference was noticed between the levels for the elastic modulus (Table 3). The elastic modulus of longitudinal PM was significantly different between fresh and flash frozen samples (17.2 ± 9 MPa against 21.3 ± 9.1 MPa respectively) (Table 3).

The CSA were used to choose the most likely CSA of tested samples from the probabilistic distribution computed from a Monte-Carlo approach of uncertainties quantification. Then the

probabilistic range of elastic moduli computed from the 38th (E_38) and 62th (E_62) percentile probabilistic values of CSA is depicted in the Table 3. The range of probabilistic values of elastic modulus differ from the standard deviation range. Indeed, the probabilistic elastic moduli range (E_32 – E_68) was greater than the range of SD experimental elastic moduli (E) for DAC samples in circumferential direction. In longitudinal direction, the inferior value of probabilistic range (E_62) was greater than the SD inferior value of DAC samples. For the PM samples in longitudinal direction, E_38 and E_62 values were respectively always greater to the superior and the inferior SD values.

Ogden coefficient presented in Table. 5 were computed for curves (min, max and typical) of the Fig. 4 and were represented in Fig. B (Appendix B).

Typical stress and strain fields were depicted in Appendix C as well as the maximum deformations to failure in Table B.1 [Appendix B]. The maximum stresses and strains are not located in the same part of the sample describing the heterogeneous behavior of the DAC and PM tissues.

4. Discussion

The elastic mechanical properties of meninges along the porcine spinal cord were quantified and tested in the longitudinal and the circumferential directions. While assuming a linear elastic behavior only provides a macroscopic mechanical description of only the linear part of the stress/stress curve. The results showed that the cervical DAC linear modulus is the lowest in longitudinal loading direction while the lumbar DAC linear modulus is the highest in circumferential loading direction. The effect of conservation method between fresh and flash frozen (at-80°C) samples at the thoracic level showed suggest the reliability of the flash frozen conservative approach for DAC tissues. To the best of our knowledge, such comparison of mechanical properties between the cervical, thoracic and lumbar spinal levels as well as of the behavior of flash frozen with fresh samples is an addition to the current literature. A probabilistic quantification of CSA was performed to estimate the effect of measurement variabilities reported for the thickness and the width, resulting in a probabilistic elastic moduli per tissue and loading direction.

For the next paragraphs, the literature comparisons were solely focused on spinal meninges mechanical properties, without any comparison with the brain meninges properties. This choice was done due to the difference of structural tissue alignments.

4.1. Spinal levels

4.1.1. Dura-Arachnoid Complex (DAC)

The significant mechanical difference between the porcine DAC elastic moduli tested in longitudinal and circumferential loading directions matched the mechanical spinal dura mater behavior previously reported in literature. However, the magnitude of our elastic moduli was lower. Our mean longitudinal elastic modulus of DAC was 1.8 times significantly superior to the circumferential elastic modulus at the thoracic spinal level while the longitudinal elastic modulus was three times significantly superior to the circumferential elastic modulus at the lumbar spinal level which is lower than literature measurements. The longitudinal over circumferential elastic moduli ratio is still coherent (Patin et al. 1996, Zarzur 1996, Runza et al. 1999, Yang et al. 2019). Then, our results in terms of elastic modulus support a longitudinal fiber alignment for the pigs, in accordance with the literature for the rat (Maikos et al. 2008), the dog (Patin et al. 1996), for the pig (Kinaci et al. 2020) and for the human (Chauvet et al. 2010). We showed elasticity variations along the canal for the DAC in longitudinal and in circumferential loading directions. The greatest elasticity in longitudinal loading direction was measured at the cervical spinal level whereas the greatest elasticity in the circumferential loading direction was measured at the lumbar level.

In longitudinal loading direction for DAC samples, significant differences were highlighted in our study between each spinal level of elastic moduli. The reported longitudinal elastic modulus at the lumbar level of human cadavers varied between 65 and 102 MPa for fresh samples (Runza et al. 1999) whereas it was 36.6±12.6 MPa in our study in similar testing conditions. A similar difference is observed between the frozen samples of human cadavers varying between 42 and 142 MPa (Runza et al. 1999) whereas it was 39.3±19.3 MPa for flash frozen samples in our study. In circumferential loading direction, the DAC elastic modulus was found significantly lower at the lumbar level in this

study when compared to cervical and thoracic levels. These differences of elasticity could be due to local structural changes at the cervical and lumbar levels in order to respectively support the longitudinal and the circumferential loading. Indeed, the particular local geometry around the foramen magnum and around the cauda equina would induce these local structural changes, locally modifying the mechanical properties. A loss of a longitudinal alignment at the cervical and the lumbar spinal levels could explain a loss of cervical longitudinal and lumbar circumferential elasticity.

Firstly, a potential link between the tissue stiffness variation and the range of motion of each spinal segment could explain such findings. Indeed, the absence of significant difference between the longitudinal and the circumferential loading orientation at the cervical level of DAC could be explained by the variation of range of motion (ROM) between the spinal segments (cervical, thoracic, lumbar). Indeed, the ROM in flexion/extension, lateral bending angles are greater at the cervical level (Wilke et al. 2011, Persson et al. 2010). The capacity to flex and to bend of the neck do not induce any significant difference of elastic mechanical properties in longitudinal and in circumferential directions. Then, the lower ROM in the thoracic and lumbar spinal levels bringing a greater stability (Wilke et al. 2011) limits the circumferential the stresses and the strains in the canal. For the dura mater, this could result in a higher capacity to be stressed in the longitudinal orientation.

Secondly, the higher values of circumferential stiffness of the DAC were found at the cervical and thoracic levels. The high or reasonable presence of cerebrospinal fluid (CSF) vortices and the higher CSF pulsatile pressure in the canal of the cervical and thoracic segments compared to the lumbar segment (Tangen et al. 2015, Khani et al. 2018) could explain such observations. Indeed, these potential stresses applied by the fluid vortices (orthogonally to the longitudinal flow direction) on the DAC in the upper spinal levels could create a tissue densification driving to a greater circumferential rigidity. This assumption takes its source from the Davis 'law (the corollary of Wolff's law for soft tissue) (Davis 1867) and from others mechanobiological theories (Liedekerke et al. 2019, Cyron and Humphrey 2017).

4.1.2. Pia Mater (PM)

In PM samples, no significant difference was observed between the elastic moduli of each spinal level. There is a limited number of studies on the PM tissue material properties compared to the dura mater. Accordingly, no comparative data was found. However, two studies investigating pia mater properties performed on ewe and rabbit model were used as partial comparative data. Our results show a significantly higher value of elastic modulus (18.4 ± 8 MPa) compared to the elastic modulus of cervical rabbit (2.4 MPa) tested with a ramp of 0.02 N/s (Ozawa et al. 2011). This difference can be explain by the inter-specie ROM, the motion strategy and the morphology between the rabbit and the porcine model. However, our values are coherent with the modulus (17 MPa) of the cervical ewe PM samples tested at strain rate of 0.05/s (Ramo et al. 2018c). Ozawa et al. (2011) showed that the rabbit pia mater increased the stiffness of the spinal cord and enhanced its shape recovery after releasing the compression on the spinal cord. The porcine PM sheath seems also maintain the oval spinal cord shape with a similar elasticity. Then the Poisson's effect of the human spinal cord (Breig and Braxton

1960, Sudres et al. 2019) could be limited by the PM mechanical properties. The PM would mitigate the stresses and strains into the spinal cord during posture changes.

4.2. Protocol aspects

4.2.1. Testing model

Due to morphological, feasibility, housing, ethical in term of accessibility to human cadavers, histological (Kinaci et al. 2020) and biomechanical considerations in term of the cervical and thoracic ROM in lateral bending and in flexion/extension (Wilke et al. 2011), this quadruped makes the most appropriate transversal models human, next to non-human primates (Schomberg et al. 2017).

4.2.2. Failure pattern aspects

One of the limitations of our protocol is the method used to cut our samples. That could generate high damaging risks, making it difficult to homogenize the dimensions of each samples. The consequence of that is with the occurrence of failure at the level of clamps in a majority of samples, induced by stress concentration by the jaws [Fig. C.5]. When failure occurred in the center of samples [Fig C.6 – B, C], we observed a difference in failure pattern between the DAC in circumferential loading and the PM in longitudinal loading. Indeed, PM appeared to be more heterogeneous with vessels more apparent while the DAC appeared more homogeneous macroscopically with an assumed longitudinal fiber organization.".

Additional stress and strain fields analyses were proposed on typical samples (Fig C.1-3). Two solutions could solve this protocol issue: cutting using the sample with a steel mechanical cutting piece (Chauvet et al. 2010) and the fastening of the sample to the clamps with a pressure sensor, thus ensuring symmetrical boundary conditions. In addition, working in an environmental chamber with CSF-like fluid could maintain moisture conditions of the sample and reproduce a more biofidelic test environment. However, those solutions would certainly induce longer protocols, worsening the *post mortem* degradation of tissues.

4.2.3. Conservative approaches

Regarding conservative method aspect, our value of elastic moduli as well as our values of damage stresses are lower than the mechanical properties provided in the literature (Runza et al. 1999). This difference could be due to the time and the choice of conservation (mean time after euthanasia: mean of 7h26 against between less than 24h and 120h of low temperature freezing). The classical freezing at -4°C seems to result in a drying of the sample and to finally increase the stiffness of the samples. Mazgajczyk et al. (2012) showed cervical stress and strain values greater than our measurements. The difference of damage or maximum stresses could be explained by the porcine species used (Yorkshire X Landrace against no detailed porcine animals), the maximum time used to perform the experiments (12h23 against 24h) and the conservation method (flash freezing at -80°C against a classical freezing method below 0°C without detail).

No significant difference was mechanically observed between the fresh and flash-frozen DAC samples' elastic moduli. This could be explained by a denser fiber of the DAC structure compared to the PM structure (Reina et al. 2020). This higher density of fibers could limit the effect of freezing at

very low temperature, in limiting the shrinkage of the matter caused by H2O presence and in limiting the quantity of fluid available in the tissue. The flash-freezing conservative approach allowed to reduce the importance of the time variable in an experimental protocol, as well as to mitigate the mechanical behavior between the flash frozen and the fresh samples. In addition, both tissues have viscoelastic properties due to their direct contact with the cerebrospinal fluid. A further study investigating the viscoelastic properties differences between fresh and flash frozen samples could highlight the effect of fluids with respect to the tissue structure in the mechanical behavior of spinal meninges. Then, the flash freezing increased the stiffness of PM samples with respect to the fresh samples. A further study could investigate this effect potentially induced by a limited number of flash-frozen PM thoracic samples.

4.2.4. Thickness uncertainty analysis

The measurements of force/displacement of the samples remain a challenge, particularly due to uncertainty errors induced by the protocol. The thickness measurements were not performed on the tested samples but on one specific porcine subject not included in the mechanical testing protocol due to the high damaging risk induces by tissue manipulation. Measurement errors from the tools as well as the difference of sample thickness measurement (with a different pig to avoid damaging the sample) could lead to non-linear result uncertainties (Appendix A – Fig. A.2). A propagation uncertainty analysis is not frequently used for soft tissue characterization, but it brings a more complete and comparable range of mechanical properties. The GUM uncertainty analysis (ISO 98:1995 GUM) provided the uncertainty distribution (Appendix A – Fig. A.1) of CSA as an output and from input uncertainty distributions of thickness and width repeatability and width resolution. Such output CSA uncertainty distribution is then used to the probabilistic elastic moduli calculations. The more the input uncertainty is clearly defined, the more the output uncertainty distribution will be accurate. As depicted in Table 3, differences between the probabilistic moduli (E_32 and E_68) and the experimental elastic modulus (E) varied with respect to the type of tissue (DAC and PM) and with respect to the loading direction (longitudinal or circumferential). When focusing on the existing available elastic moduli values in the literature, no uncertainties are provided and the provided SD ranges of experimental elastic moduli should then be taken carefully.

To experimentally face the thickness measurement challenge, the implementation of a non-contact measurement method (laser) during the tensile test could be investigated. Otherwise, a combined approach between geometrical and biomechanical experiments would allow to establish potential correlation between geometrical and biomechanical behavior of the meninges as proposed by Yoganandan et al. (2000) for the cervical human ligaments.

4.2.5. Strain rate and linear elasticity approximation

Only one moderate strain rate (0.2 mm/s) was used to describe the mechanical properties of the spinal meninges along the spinal cord which would correspond to a value lower than those occurring during injury [Ramo et al. 2018b].

Previously reported uniaxial tensile tests showed no significant strain rate dependency at low strain rate and moderate strain rates (0.01s-1, 0.1s-1 and 1s-1) for dura mater [Persson et al.2010]. The same finding was reported for the pia-arachnoid complex at 0.016 and 0.16 s-1 [Ramo et al. 2018c]. However, strain dependency of the meninges should be investigated more in details in future work. In addition, the elastic properties are easily comparable with the existing literature [Zwirner et al. 2019, Runza et al. 1999, Ramo et al. 2018c, Ozawa et al. 2011]. A potential correlation between "the higher nonlinearity observed in the circumferential direction as compared to longitudinal direction" due to the deformation of the toe region and the low deformations of the spinal cord in physiological conditions. gradual to region due to the toe region during physiological motion of the spinal cord was discussed in literature [Shetye et al. 2014]. We assumed the linear part would be a transitional phase (between the physiological behavior of the tissue and a beginning failure phase) in which the tissue is not yet injured. We additionally provided a range of isotropic hyperelastic (one term Ogden model) coefficients to provide a better description of the tissue behavior in all test loadings direction for the first 15% of strain.

The μ Ogden coefficients of the typical curves were found superior to those provided for spinal bovine dura mater at 0.01 s-1 (5.0 MPa against almost null in the longitudinal direction and 2.4 MPa against 2.2 MPa in the circumferential direction respectively) . The b Ogden coefficients were found inferior to those provided in the same study (11.9 against almost 24.0 in the longitudinal direction and 10.5 against 18.0 in the circumferential direction respectively) [Persson et al. 2010]. No equivalent data was found to compare the Ogden coefficients of PM.

Trends reported in inter-segmental spinal level variation (cervical, thoracic and lumbar) of elastic properties in DAC and PM need to be confirmed due to high standard error induced by within-subject and between-subject variability. Thus a larger population of samples by levels and by subject will be tested. Anisotropic hyperelastic models [De Kegel et al. 2018, Shetye et al. 2014] as well as dorsal and ventral locations of samples along the spine [Mazgajczyk et al. 2012] could be investigated in future work. Finally, our mechanical properties could be used in spine FE models such as stenotic scenarios [Bailly et al. 2020] or post-surgery analysis [Stoner et al. 2020] for a better description of tissues in longitudinal and circumferential loading direction of DAC and in longitudinal PM.

5. Conclusion

The porcine model is an appropriate alternative to study the mechanical properties of meninges compared to human cadavers. In addition, this study provided isotropic hyperelastic properties and showed the negligible effect of a flash freezing conservative method to provide comparable results on DAC tissues, thus limiting the effect of the time factor in such experimental protocol.

The following mean values were proposed for the elastic moduli of the spinal meninges:

- Longitudinal DAC elastic moduli: **22.4 MPa** (SE: 23.0) in cervical, **38.1 MPa** (SE: 23.3) in thoracic and **36.6 MPa** (SE: 23.81) in lumbar spinal levels.
- Circumferential DAC elastic moduli: **20.6 MPa** (SE: 6.6) in cervical, **21.2 MPa** (SE: 6.7) in thoracic and **12.2 MPa** (SE: 6.6) in lumbar spinal levels.
- Longitudinal PM elastic moduli: **18.4 MPa** (SE: 14.4) in cervical, **17.2 MPa** (SE: 13.7) in thoracic and **19.6 MPa** (SE: 13.5) in lumbar spinal levels.

This variety of mechanical properties of the meninges suggests that it cannot be regarded as a homogenous structure along the whole length of the spinal cord. Furthermore, a spatial personalization along the spinal cord of this biological soft elastic behavior should be taken into account when building a numerical model of the central nervous system.

6. Acknowledgements

The authors wish to thank Elisabeth Laroche for the technical assistance during the experiments.

7. Funding

This research was funded by Aix-Marseille University PhD scholarship and by the Franco-Quebec research grant “Samuel-De Champlain”.

		Fresh samples			Flash Frozen samples		
Level	**Tissue**	**Nb of tested samples**	**Nb of excluded**	**Nb of analyzed**	**Nb of tested samples**	**Nb of excluded**	**Nb of analyzed**
Cervical	**LONG DAC**	15	1	14		X	
	CIRC DAC	20	3	17		X	
	LONG PM	14	0	14		X	
Thoracic	**LONG DAC**	15	3	12	9	3	6
	CIRC DAC	8	0	8	11	0	11
	LONG PM	18	1	17	13	5	8
Lumbar	**LONG DAC**	10	0	10		X	
	CIRC DAC	12	1	11		X	
	LONG PM	16	0	16		X	
Total	**LONG DAC**	40	4	36	9	3	6
	CIRC DAC	40	4	36	11	0	11
	LONG PM	48	1	47	13	5	8
Total		128	9	119	33	8	25

Table 1. Summarized description of number of samples

Level	**Tissue**	**Length [mm]**	**Width [mm]**	**Thickness [mm]**	**Cross-sectional area [mm²]**
Cervical	**LONG DAC**	9.65 (0.96) [8.33-12.06]	11.35 (2.22) [8.1-15.73]	0.28 (0.05) [0.22-0.37]	3.18 (0.62) [2.27-4.40]
	CIRC DAC	10.61 (1.95) [8.19-15.92]	11.16 (2.75) [7.2-15.02]	0.28 (0.05) [0.22-0.37]	3.12 (0.77) [2.02-4.21]
	LONG PM	9.1 (1.7) [6.99-12.7]	8.09 (1.93) [3.96-10.92]	0.22 (0.04) [0.16-0.28]	1.78 (0.42) [0.87-2.40]
Thoracic	**LONG DAC**	11.7 (1.81) [9.23-15.36]	11.79 (4.6) [7.66-22.44]	0.32 (0.05) [0.19-0.49]	3.77 (1.47) [2.45-7.18]
	CIRC DAC	11.18 (2.22) [9.14-15.6]	15.12 (3.62) [9.34-20.98]	0.32 (0.05) [0.19-0.49]	4.84 (1.16) [2.99-6.71]
	LONG PM	10.65 (1.61) [8.1-13.75]	12.13 (3.75) [4.5-16.21]	0.2 (0.05) [0.11-0.29]	2.44 (0.76) [0.90-3.24]
Lumbar	**LONG DAC**	12.35 (1.92) [10.08-15.49]	9.64 (1.69) [7.94-12.57]	0.28 (0.05) [0.21-0.37]	2.7 (0.47) [2.22-3.52]
	CIRC DAC	11.36 (3.44) [6.36-18.51]	12.03 (3.01) [6.88-6.69]	0.28 (0.05) [0.21-0.37]	3.37 (0.84) [1.93-4.67]
	LONG PM	11.13 (2.14) [6.23-13.91]	8.88 (2.35) [4.79-12.55]	0.2 (0.04) [0.14-0.28]	1.78 (0.47) [0.96-2.51]

Table 2. Summary of sample dimensions. Each quantity is described as the mean value, the standard deviation between parenthesis and the min and max respectively, between brackets.

Level	**Tissue**	**Toe strain (ε *toe*)**	**Toe stress (σ *toe*) [MPa]**	**Failure strain (ε *failure*)**	**Failure stress (σ *failure*) [MPa]**	**Elastic modulus (E) [MPa]**	**E_0.32 [MPa]**	**E_0.68 [MPa]**
Cervical	**LONG DAC (n=14)**	0.04 (0,03)*T	0.5 (0.21)	0.25 (0.09)*T,L	5.08 (2.97)	22.3 (10.0)*T,L (SE: 23.0)	30.3	17.4
	CIRC DAC (n=17)	**0.04 (0.02)**	0.49 (0.37)	**0.23 (0.1)*L**	**4.1 (2.23)**	**20.6 (8.1)*L** (SE: 6.6)	**49.5**	**25.8**

	LONG PM (n=14)	**0.03 (0.01)*T,L**	**0.64 (0.27)*T,L**	0.23 (0.08)	3.85 (1.88)	18.4 (8.0) (SE: 14.4)	30.4	16.0
Thoracic	**LONG DAC (n=12)**	**0.02 (0.01)*C**	0.49 (0.33)	0.15 (0.09)*C	4.98 (2.7)	38.1 (12.6)*C,§ (SE: 23.3)	69.1	27.4
	CIRC DAC (n=8)	**0.03 (0.01)**	0.27 (0.07)	**0.21 (0.08)*L**	**3.94 (1.38)*L**	**21.2 (3.0)*L,§** (SE: 6.7)	**30.4**	**16.6**
	LONG PM (n=17)	0.02 (0.02)*C	0.34 (0.18)*C	0.2 (0.05)	3.07 (1.73)	17.2 (9) (SE: 13.7)	28.4	11.6
Lumbar	**LONG DAC (n=10)**	**0.03 (0.01)**	0.73 (0.41)	0.18 (0.09)*C	5.3 (1.62)	36.6 (12.6)*C,§ (SE: 23.8)	45.2	26.8
	CIRC DAC (n=11)	**0.03 (0.01)**	0.3 (0.11)	**0.32 (0.14)*C,T**	**3.26 (0.89)*T**	**12.2 (4.4)*C,T,§** (SE: 6.6)	**17.2**	**8.9**
	LONG PM (n=16)	**0.02 (0.01)*C**	**0.43 (0.2)*C**	0.18 (0.03)	3.17 (0.91)	19.6 (6.8) (SE: 13.5)	31.1	15.2
Total	**LONG DAC (n=36)**	0.03 (0,02)	0.56 (0.32)	0.2 (0.1)	5.11 (2.5)	32.3 (13.5) (SE: 21.7)		
	CIRC DAC (n=36)	0.03 (0,02)	0.38 (0.28)	0.25 (0.12)	3.81 (1.74)	18.0 (7.3) (SE: 6.53)		
	LONG PM (n=47)	0.02 (0,01)	0.46 (0.25)	0.2 (0.06)	3.34 (1.56)	18.4 (7.9) (SE: 10.2)		

Mean with standard deviation in parenthesis values as well as reported standard error (SE).
Bold*C,T,L stand for a significant difference between the spinal level and the level given by the letters C (cervical),T (thoracic) or L (lumbar) for a given tissue and a given variable. ($p<0.05$)
Bold § stands for a significant difference between the DAC longitudinal and circumferential for a given spinal level ($p<0.05$).
Table 3. Summary of post-processed quantities by spinal segment (stress, strain, elastic moduli and probabilistic elastic moduli) for toe region, quasi-linear region and damage region.

Level	**Tissue**	**Elastic Modulus [MPa]**	
		Fresh samples	**Flash Frozen samples**
Thoracic	**LONG DAC**	38.1 (12.6) n=12	39.3 (19.3) n=6
	CIRC DAC	21.2 (3) n=8	17.4 (4.4) n=11
	LONG PM	**17.2 (9) n=17**	**21.3 (9.1) n=5**

Bold* stands for a significant difference between the fresh and the flash-freezing samples for the thoracic level and a given tissue ($p<0.05$).
Table 4. Comparison table of samples's elastic modulus between fresh and flash-freezing conservation methods.

Authors	Journal	Number of specimen ; samples	Specie	Tissue	Spinal level	Type of test	Strain rates	Conservation method	Elastic modulus	
									Longitudinal	Transverse
Patin *et al.* 1993	Anesthesia & Analgesia	9 specimens ; 7 samples by specie	human dog	dura mater	lumbar	uniaxial tension	1.67 mm/s	Refrigerated in saline solution	human : 138 - 265 MPa dog : 58.8 - 73.5 MPa	human : 7.8 - 76.4 MPa dog : 54.9 - 58.8 MPa
Runza *et al.* 1999	Anesthesia & Analgesia	6 cadavers ;	human bovin	dura mater	T12 - L4/L5	uniaxial tension	10 mm/min	In saline solution , frozen at 4°C for 24h and 120h	human : 65 - 102 MPa bovin : 25 - 80 MPa	human : 5 MPa
Maikos *et al*. 2008	Journal of Neurotrauma	23 spinal samples	rat	dura mater	C1 - L1	uniaxial tension	19.4 sec-1; 0.0014 sec-1	2h after sacrifice		
Mazgajczyk *et al.* 2012	Acta of bioengineering and biomechanic	9 specimens ; 250 samples	porcine	dura mater	C1 - C7	uniaxial tension	2 mm/min	Frozen		
Chauvet *et al.* 2010	Neurosurgical Review	10 specimens; 22 samples	human	dura mater	Craniocervical junction	uniaxial tension		Fresh cadaver	entire dura : 44 - 91 MPa split dura : 19 - 25 MPa	
Yang *et al.* 2019	Zhongguo Xiu Fu Chong Jian Wai Ke Za Zhi	5 specimens	sheep	dura mater	C6, C7, T11, T12, L4, and L5	uniaxial tension	0.016 mm/s	in saline solution	cervical : 15.97±2.52 MPa thoracic : 12.39±1.88 MPa lumbar : 8.33 ±3.10 MPa	cervical : 14.38±2.68 MPa thoracic : 8.78±1.01 MPa lumbar : 3.46±1.24 MPa
Ozawa *et al.* 2011	Journal of Neurosurgery	9 specimens	rabbit	pia mater	C5 - C6	uniaxial tension and compression	0.02 N/s	In saline solution	2.4 MPa	
Ramo *et al.* 2018c	Acta Biomaterialia	8 specimens	ewe	pia-arachnoid complex	C0 - C7	uniaxial tension	0.05sec-1	fresh after sacrifice	17 MPa	

Table 5. Comparative literature table of mechanical characterization of spinal meninges

Loading direction/ Tissue	mu	b	R^2	RMSE
Longitudinal DAC				
Curve 1 (superior limit of the corridor)	6.619 (6.452, 6.787)	11.8 (11.36, 12.24)	0.9974	0.0739
Curve 2 (typical curve)	5.02 (4.882, 5.158)	11.93 (11.45, 12.41)	0.9966	0.0613
Curve 3 (inferior limit of the corridor)	3.286 (2.966, 3.606)	-7.291 (-16.47, 1.888)	0.9916	0.0292
Circumferential DAC				
Curve 1 (superior limit of the corridor)	4.684 (4.562, 4.806)	6.955 (6.379, 7.531)	0.9973	0.0396
Curve 2 (typical curve)	2.499 (2.397, 2.6)	10.5 (9.761, 11.24)	0.9942	0.0377
Curve 3 (inferior limit of the corridor)	0.765 (0.74, 0.79)	10.77 (10.18, 11.36)	0.9946	0.0109
Longitudinal PM				
Curve 1 (superior limit of the corridor)	14.12 (13.88, 14.36)	7.342 (6.972, 7.712)	0.9984	0.0885
Curve 2 (typical curve)	4.184 (4.04, 4.329)	9.01 (8.338, 9.683)	0.9966	0.0437
Curve 3 (inferior limit of the corridor)	3.763 (3.684, 3.842)	2.549 (1.927, 3.172)	0.9977	0.0235

Table 6. One degree Ogden model material constants b and mu the shear modulus of the curves depicted in Fig. 4 and Fig. B (Appendix B). A 95% confidence interval is provided between parenthesis for each couple of the material constants.

8. References

1. Bailly, N., Diotalevi, L., Beauséjour, M.-H., Wagnac, É., Mac-Thiong, J.-M., Petit, Y., 2020. Numerical investigation of the relative effect of disc bulging and ligamentum flavum hypertrophy on the mechanism of central cord syndrome. Clinical Biomechanics 74, 58–65. https://doi.org/10.1016/j.clinbiomech.2020.02.008
2. Bertram, C.D., Heil, M., 2016. A Poroelastic Fluid/Structure-Interaction Model of Cerebrospinal Fluid Dynamics in the Cord With Syringomyelia and Adjacent Subarachnoid-Space Stenosis. J Biomech Eng 139, 011001-011001–10. https://doi.org/10.1115/1.4034657
3. Breig, A., & Braxton, V. (1960). Biomechanics of the central nervous system : some basic normal and pathologic phenomena (book). Uppsala: Almqvist & Wiksell.
4. Bilston, L.E., Thibault, L.E., 1995. The mechanical properties of the human cervical spinal cordIn Vitro. Ann Biomed Eng 24, 67–74. https://doi.org/10.1007/BF02770996
5. Brummund, M., Brailovski, V., Petit, Y., Facchinello, Y., Mac-Thiong, J.-M., 2017. Impact of anchor type on porcine lumbar biomechanics: Finite element modelling and in-vitro validation. Clinical Biomechanics 43, 86–94. https://doi.org/10.1016/j.clinbiomech.2017.02.007
6. Chauvet, D., Carpentier, A., Allain, J.-M., Polivka, M., Crépin, J., George, B., 2010. Histological and biomechanical study of dura mater applied to the technique of dura splitting decompression in Chiari type I malformation. Neurosurg Rev 33, 287–295. https://doi.org/10.1007/s10143-010-0261-x
7. Cyron, C.J., Humphrey, J.D., 2017. Growth and Remodeling of Load-Bearing Biological Soft Tissues. Meccanica 52, 645–664. https://doi.org/10.1007/s11012-016-0472-5
8. Czyż, M., Ścigała, K., Będziński, R., Jarmundowicz, W., 2012. Finite element modelling of the cervical spinal cord injury -- clinical assessment. Acta Bioeng Biomech 14, 23–29.
9. Davis H. G., 1867. Conservative Surgery: As Exhibited in Remedying Some of the Mechanical Causes that Operate ... D. Appleton & company.
10. Fabris, G., M. Suar, Z., Kurt, M., 2019. Micromechanical heterogeneity of the rat pia-arachnoid complex. Acta Biomaterialia 100, 29–37. https://doi.org/10.1016/j.actbio.2019.09.044
11. Fradet, L., Arnoux, P.-J., Callot, V., Petit, Y., 2016. Geometrical variations in white and gray matter affect the biomechanics of spinal cord injuries more than the arachnoid space. Advances in Mechanical Engineering 8, 1687814016664703. https://doi.org/10.1177/1687814016664703
12. Fradet, L., Cliche, F., Petit, Y., Mac-Thiong, J.-M., Arnoux, P.-J., 2016. Strain rate dependent behavior of the porcine spinal cord under transverse dynamic compression. Proc Inst Mech Eng H 230, 858–866. https://doi.org/10.1177/0954411916655373
13. Fountoulakis, M., Hardmeier, R., Höger, H., Lubec, G., 2001. Postmortem Changes in the Level of Brain Proteins. Experimental Neurology 167, 86–94. https://doi.org/10.1006/exnr.2000.7529
14. Garo, A., Hrapko, M., van Dommelen, J. a. W., Peters, G.W.M., 2007. Towards a reliable characterisation of the mechanical behaviour of brain tissue: The effects of post-mortem time and sample preparation. Biorheology 44, 51–58.
15. Henao, J., Aubin, C.-É., Labelle, H., Arnoux, P.-J., 2016. Patient-specific finite element model of the spine and spinal cord to assess the neurological impact of scoliosis correction: preliminary application on two cases with and without intraoperative neurological complications. Computer Methods in Biomechanics and Biomedical Engineering 19, 901–910. https://doi.org/10.1080/10255842.2015.1075010

16. ISO 98:1995 Guide to the expression of Uncertainty in Measurement 2nd edn (1995) International Organization for Standardization, Geneva
17. JCGM 101:2008 Evaluation of measurement data – Supplement 1 to the "Guide to the expression of uncertainty in measurement" – Propagation of distributions using a Monte Carlo method (2008) Sèvres, France: BIPM Joint Committee for Guides in Metrology
18. Khani, M., Sass, L.R., Xing, T., Keith Sharp, M., Balédent, O., Martin, B.A., 2018. Anthropomorphic Model of Intrathecal Cerebrospinal Fluid Dynamics Within the Spinal Subarachnoid Space: Spinal Cord Nerve Roots Increase Steady-Streaming. J Biomech Eng 140. https://doi.org/10.1115/1.4040401
19. Khuyagbaatar, B., Kim, K., Hyuk Kim, Y., 2014. Effect of bone fragment impact velocity on biomechanical parameters related to spinal cord injury: A finite element study. Journal of Biomechanics 47, 2820–2825. https://doi.org/10.1016/j.jbiomech.2014.04.042
20. Kim, K.-T., Streijger, F., So, K., Manouchehri, N., Shortt, K., Okon, E.B., Tigchelaar, S., Fong, A., Morrison, C., Keung, M., Sun, J., Liu, E., Cripton, P.A., Kwon, B.K., 2019. Differences in Morphometric Measures of the Uninjured Porcine Spinal Cord and Dural Sac Predict Histological and Behavioral Outcomes after Traumatic Spinal Cord Injury. Journal of Neurotrauma 36, 3005–3017. https://doi.org/10.1089/neu.2018.5930
21. Kimpara, H., Nakahira, Y., Iwamoto, M., Miki, K., Ichihara, K., Kawano, S., Taguchi, T., 2006. Investigation of anteroposterior head-neck responses during severe frontal impacts using a brain-spinal cord complex FE model. Stapp Car Crash J 50, 509–544.
22. Kinaci, A., Bergmann, W., Bleys, R.L., van der Zwan, A., van Doormaal, T.P., 2020. Histologic Comparison of the Dura Mater among Species. Comparative Medicine 70, 170–175. https://doi.org/10.30802/AALAS-CM-19-000022
23. Lévy, S., Baucher, G., Roche, P.-H., Evin, M., Callot, V., Arnoux, P.-J., 2020. Biomechanical comparison of spinal cord compression types occurring in Degenerative Cervical Myelopathy. Clinical Biomechanics 105174. https://doi.org/10.1016/j.clinbiomech.2020.105174
24. Liedekerke, P.V., Neitsch, J., Johann, T., Alessandri, K., Nassoy, P., Drasdo, D., 2019. Quantitative cell-based model predicts mechanical stress response of growing tumor spheroids over various growth conditions and cell lines. PLOS Computational Biology 15, e1006273. https://doi.org/10.1371/journal.pcbi.1006273
25. Maikos, J.T., Elias, R.A.I., Shreiber, D.I., 2008. Mechanical Properties of Dura Mater from the Rat Brain and Spinal Cord. Journal of Neurotrauma 25, 38–51. https://doi.org/10.1089/neu.2007.0348
26. Mazgajczyk, E., Ścigała, K., Czyż, M., Jarmundowicz, W., Będziński, R., 2012. Mechanical properties of cervical dura mater. Acta Bioeng Biomech 14, 51–58.
27. Mazuchowski, E, Thibault, L. Biomechanical properties of the human spinal cord and pia mater, 2003, http://www.tulane.edu/sbc2003/pdfdocs/1205.PDF
28. Ozawa, H., Matsumoto, T., Ohashi, T., Sato, M., Kokubun, S., 2004. Mechanical properties and function of the spinal pia mater. Journal of Neurosurgery: Spine 1, 122–127. https://doi.org/10.3171/spi.2004.1.1.0122
29. Patin, D., Eckstein, E., Harum, K., Pallares, V., 1993. Anatomic and Biomechanical Properties of Human Lumbar Dura Mater. Anesthesia & Analgesia 76, 535–540.
30. Persson, C., Evans, S., Marsh, R., Summers, J.L., Hall, R.M., 2010. Poisson's Ratio and Strain Rate Dependency of the Constitutive Behavior of Spinal Dura Mater. Ann Biomed Eng 38, 975–983. https://doi.org/10.1007/s10439-010-9924-6
31. R Core Team (2018). R: A language and environment for statistical computing. R Foundation for Statistical Computing, Vienna, Austria. URL https://www.R-project.org/.

32. Ramo, N., Shetye, S.S., Puttlitz, C.M., 2018. Damage Accumulation Modeling and Rate Dependency of Spinal Dura Mater. ASME J of Medical Diagnostics 1. https://doi.org/10.1115/1.4038261
33. Ramo, N.L., Shetye, S.S., Streijger, F., Lee, J.H.T., Troyer, K.L., Kwon, B.K., Cripton, P., Puttlitz, C.M., 2018. Comparison of In-Vivo and Ex-Vivo Viscoelastic Behavior of the Spinal Cord. Acta Biomater 68, 78–89. https://doi.org/10.1016/j.actbio.2017.12.024
34. Ramo, N.L., Troyer, K.L., Puttlitz, C.M., 2018. Viscoelasticity of spinal cord and meningeal tissues. Acta Biomaterialia 75, 253–262. https://doi.org/10.1016/j.actbio.2018.05.045
35. Reina, M., Dittmann, M., Garcia, A., Vanzundert, A., 1997. New perspectives in the microscopic structure of human dura mater in the dorsolumbar region. Regional Anesthesia and Pain Medicine 22, 161–166. https://doi.org/10.1016/S1098-7339(06)80036-2
36. Reina, M.A., Boezaart, A., De Andres-Serrano, C., Rubio-Haro, R., De Andrés, J., 2020. Microanatomy Relevant to Intrathecal Drug Delivery, in: Jain, K.K. (Ed.), Drug Delivery Systems, Methods in Molecular Biology. Springer, New York, NY, pp. 109–120. https://doi.org/10.1007/978-1-4939-9798-5_4
37. Runza, M., Pietrabissa, R., Mantero, S., Albani, A., Quaglini, V., Contro, R., 1999. Lumbar Dura Mater Biomechanics: Experimental Characterization and Scanning Electron Microscopy Observations. Anesthesia & Analgesia 88, 1317–1321. https://doi.org/10.1213/00000539-199906000-00022
38. Sakka, L., Gabrillargues, J., Coll, G., 2016. Anatomy of the Spinal Meninges. Oper Neurosurg (Hagerstown) 12, 168–188. https://doi.org/10.1227/NEU.0000000000001048
39. Schomberg, D.T., Miranpuri, G.S., Chopra, A., Patel, K., Meudt, J.J., Tellez, A., Resnick, D.K., Shanmuganayagam, D., 2017. Translational Relevance of Swine Models of Spinal Cord Injury. J. Neurotrauma 34, 541–551. https://doi.org/10.1089/neu.2016.4567
40. Shetye, S.S., Deault, M., Puttlitz, C.M., 2014. Biaxial Response of Ovine Spinal Cord Dura Mater. J Mech Behav Biomed Mater 34, 146–153. https://doi.org/10.1016/j.jmbbm.2014.02.014
41. Solaguren-Beascoa Fernández, M., Alegre Calderón, J.M., Bravo Díez, P.M., 2009. Implementation in MATLAB of the adaptive Monte Carlo method for the evaluation of measurement uncertainties. Accred Qual Assur 14, 95–106. https://doi.org/10.1007/s00769-008-0475-6
42. Sparrey, C.J., Keaveny, T.M., 2009. The Effect of Flash Freezing on Variability in Spinal Cord Compression Behavior. J Biomech Eng 131. https://doi.org/10.1115/1.4000079
43. Stoner, K.E., Abode-Iyamah, K.O., Fredericks, D.C., Viljoen, S., Howard, M.A., Grosland, N.M., 2020. A comprehensive finite element model of surgical treatment for cervical myelopathy. Clinical Biomechanics 74, 79–86. https://doi.org/10.1016/j.clinbiomech.2020.02.009
44. Sudres, P., Evin, M., Arnoux, P.-J., Callot, V., 2020. Cervical canal morphology: Effects of neck flexion in normal condition - New elements for biomechanical simulations and surgical management. Spine Publish Ahead of Print. https://doi.org/10.1097/BRS.0000000000003496
45. Swindle, M.M., Smith, A.C., 2013. Best Practices for Performing Experimental Surgery in Swine. Journal of Investigative Surgery 26, 63–71. https://doi.org/10.3109/08941939.2012.693149
46. Tangen, K.M., Hsu, Y., Zhu, D.C., Linninger, A.A., 2015. CNS wide simulation of flow resistance and drug transport due to spinal microanatomy. Journal of Biomechanics 48, 2144–2154. https://doi.org/10.1016/j.jbiomech.2015.02.018
47. Tirrell, T.F., Rademaker, A.W., Lieber, R.L., 2018. Analysis of hierarchical biomechanical data structures using mixed-effects models. Journal of Biomechanics 69, 34–39. https://doi.org/10.1016/j.jbiomech.2018.01.013

48. Vandenabeele, F., Creemers, J., Lambrichts, I., 1996. Ultrastructure of the human spinal arachnoid mater and dura mater. J Anat 189, 417–430.
49. Wilke, H.-J., Geppert, J., Kienle, A., 2011. Biomechanical in vitro evaluation of the complete porcine spine in comparison with data of the human spine. Eur Spine J 20, 1859–1868. https://doi.org/10.1007/s00586-011-1822-6
50. Yang, C., Yang, X., Lan, X., Zhang, H., Wang, M., Zhang, Y., Xu, Y., Zhen, P., 2019. [Structure and mechanical characteristics of spinal dura mater in different segments of sheep's spine]. Zhongguo Xiu Fu Chong Jian Wai Ke Za Zhi 33, 232–238. https://doi.org/10.7507/1002-1892.201807085
51. Yoganandan, N., Kumaresan, S., Pintar, F.A., 2000. Geometric and Mechanical Properties of Human Cervical Spine Ligaments. J Biomech Eng 122, 623–629. https://doi.org/10.1115/1.1322034
52. Zarzur, E., 1996. Mechanical properties of the human lumbar dura mater. Arquivos de Neuro-Psiquiatria 54, 455–460. https://doi.org/10.1590/S0004-282X1996000300015
53. Zwirner, J., Scholze, M., Waddell, J.N., Ondruschka, B., Hammer, N., 2019. Mechanical Properties of Human Dura Mater in Tension – An Analysis at an Age Range of 2 to 94 Years. Sci Rep 9, 1–11. https://doi.org/10.1038/s41598-019-52836-9

Figures

Figure 1. Mechanical testing set up: A/ (1) Sandpaper support with (2) fastened sample (left), with stochastic pattern (right) ; B/ Ramp test to-failure. (3) Clamps, (4) load cell ; C/ Lateral view of the setup with (5) a spotlight, (6) a white filter for indirect lightening of the sample ; D/ Front view including the (7) mechanical testing machine, (8) a high-definition camera, (9) a sliding support to adjust the location of the camera and (10) a computer to control and to record the measurement.

Figure 2. Typical imposed displacement over time for each mechanical tensile test. 1) Initial pre-load, 2) 30 preconditioning cycles, 3) ramp to failure.

Figure 3. Identification of the linear elastic region of interest. A- force/displacement responses with two elastic limits delimiting the three regions (1 - toe region ending by the toe force and the toe displacement, 2 – linear elastic region, 3 – failure region starting by the failure force and the failure displacement) and the linear regression, B) 2nd derivative of the force/displacement curve identifying the elastic limits points.

Figure 4. Mechanical of the tissue samples (shaded and curves): A - longitudinal DAC ; B - circumferential DAC ; C - longitudinal PM). Dotted lines represent the maximum and the minimum stress/strain curves delineating the experimental corridor (shaded area) and the continuous lines represent the typical stress/strain curves for A, B and C.

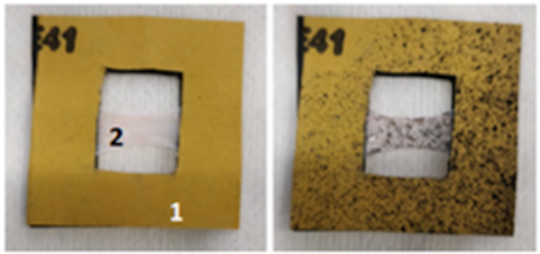

A

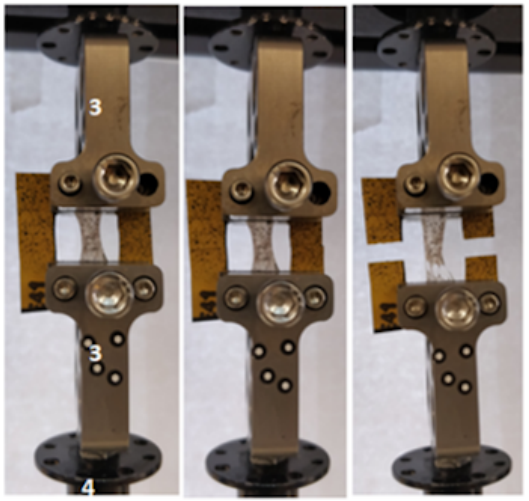

B

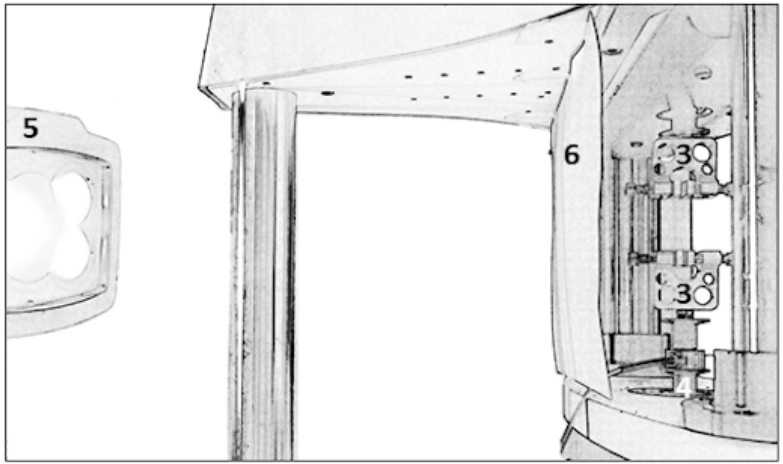

C

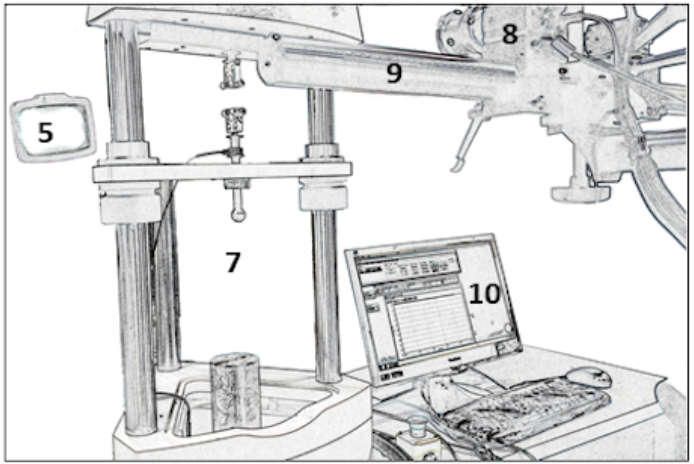

D

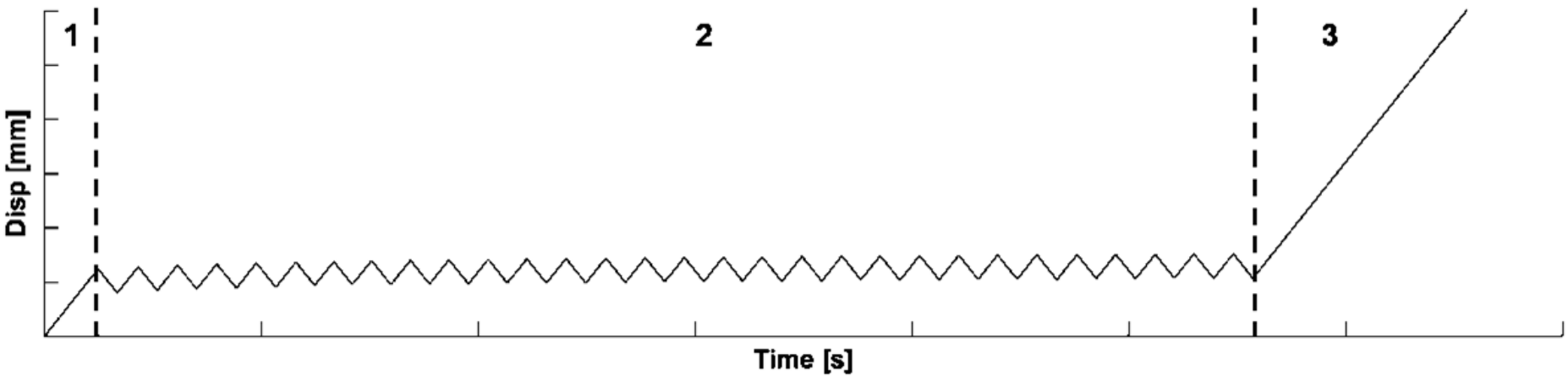
1
2
3
Disp [mm]
Time [s]

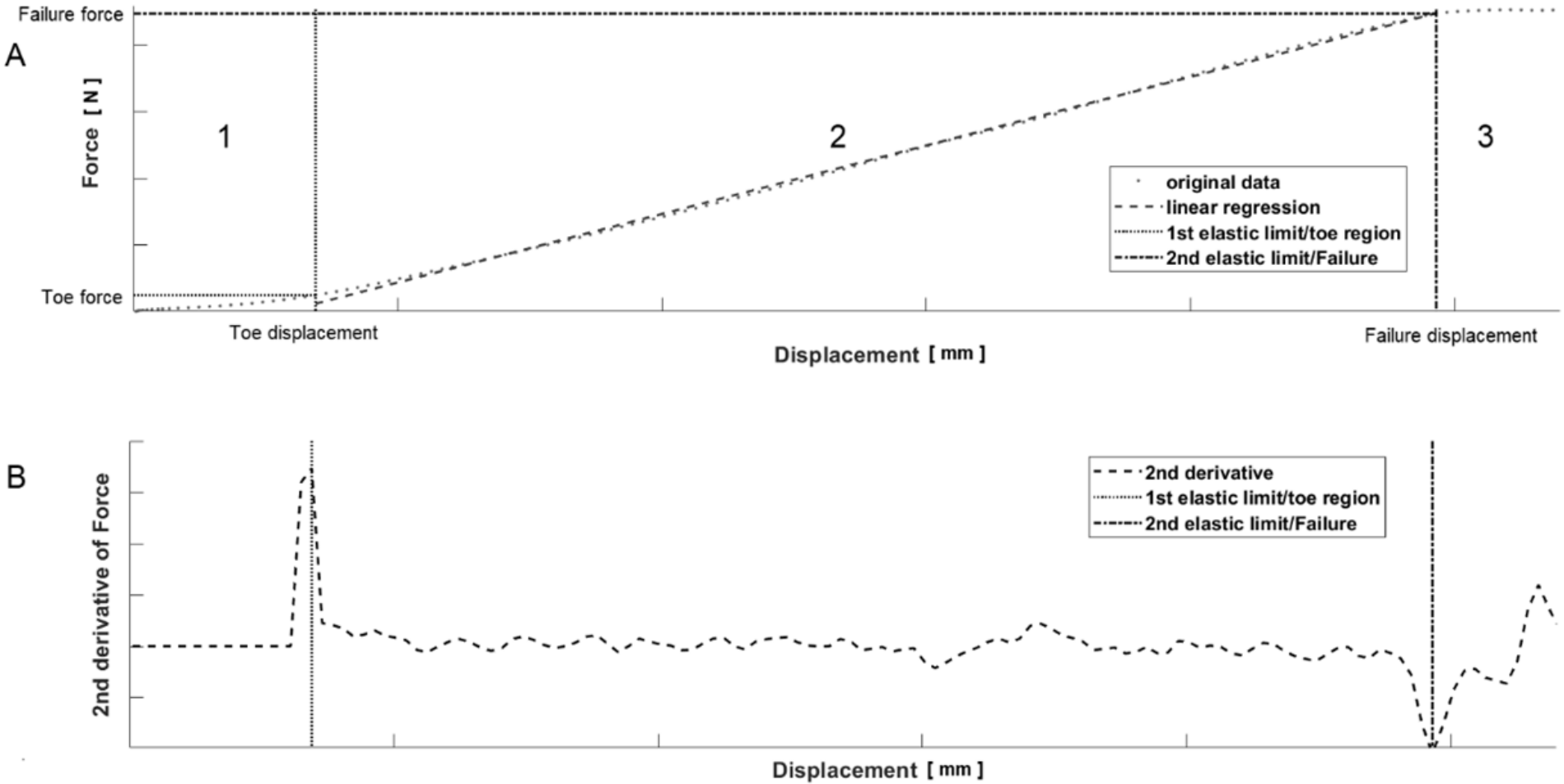
A
Failure force
Toe force
Force [N]
1
2
3
original data
linear regression
1st elastic limit/toe region
2nd elastic limit/Failure
Toe displacement
Failure displacement
Displacement [mm]
B
2nd derivative of Force
2nd derivative
1st elastic limit/toe region
2nd elastic limit/Failure
Displacement [mm]

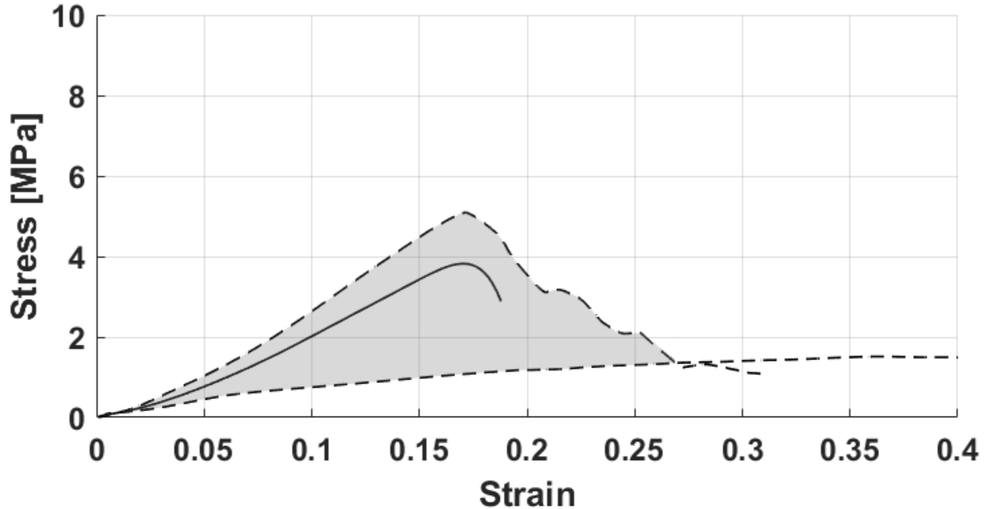
Stress [MPa]
Strain
0
2
4
6
8
10
0
0.05
0.1
0.15
0.2
0.25
0.3
0.35
0.4

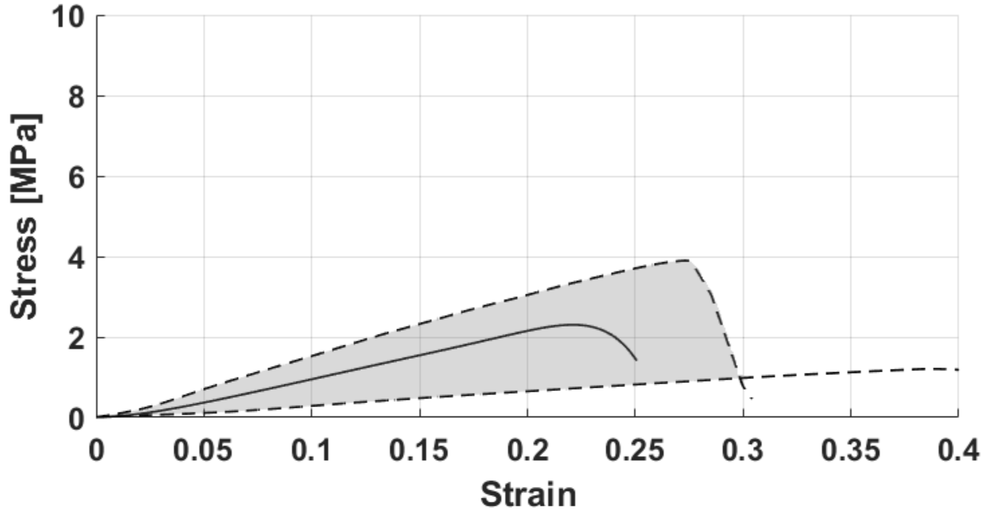
Stress [MPa]
Strain
0
2
4
6
8
10
0
0.05
0.1
0.15
0.2
0.25
0.3
0.35
0.4

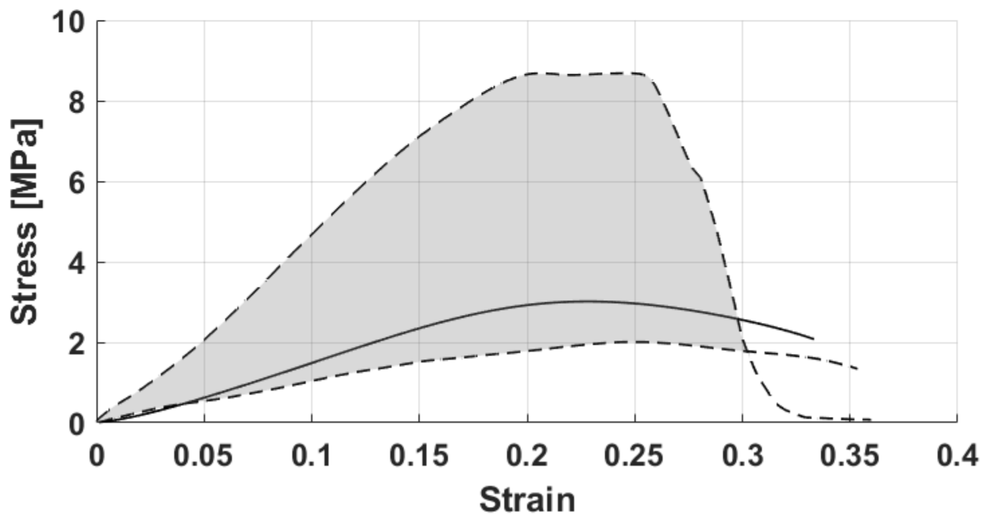
Stress [MPa]
Strain
0
2
4
6
8
10
0
0.05
0.1
0.15
0.2
0.25
0.3
0.35
0.4

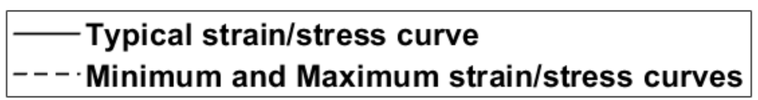
Typical strain/stress curve
Minimum and Maximum strain/stress curves

Dissection and preparation

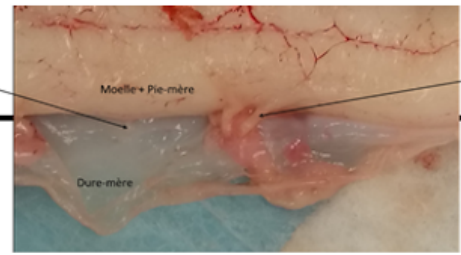

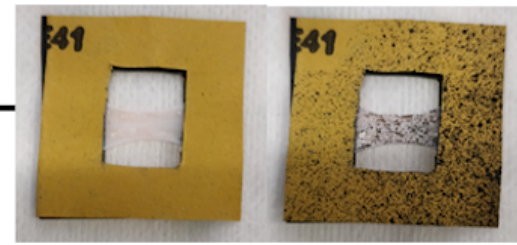

Tensile mechanical test